

# Early emergence of anthropogenically forced heat waves in the western United States and Great Lakes

Hosmay Lopez <sup>1,2\*</sup>, Robert West<sup>3</sup>, Shenfu Dong<sup>2</sup>, Gustavo Goni<sup>2</sup>, Ben Kirtman<sup>1</sup>, Sang-Ki Lee <sup>2</sup> and Robert Atlas<sup>2</sup>

**Climate projections for the twenty-first century suggest an increase in the occurrence of heat waves. However, the time at which externally forced signals of anthropogenic climate change (ACC) emerge against background natural variability (time of emergence (ToE)) has been challenging to quantify, which makes future heat-wave projections uncertain. Here we combine observations and model simulations under present and future forcing to assess how internal variability and ACC modulate US heat waves. We show that ACC dominates heat-wave occurrence over the western United States and Great Lakes regions, with ToE that occurred as early as the 2020s and 2030s, respectively. In contrast, internal variability governs heat waves in the northern and southern Great Plains, where ToE occurs in the 2050s and 2070s; this later ToE is believed to be a result of a projected increase in circulation variability, namely the Great Plain low-level jet. Thus, greater mitigation and adaptation efforts are needed in the Great Lakes and western United States regions.**

According to the US natural hazard statistics for 2015, extreme heat has been the leading weather-related cause of death in the United States for the past 30 years. A few examples of deadly heat waves worldwide include the 1980 heat wave over the US Midwest and Southern Plains<sup>1,2</sup> (1,700 fatalities), the 1995 event in Chicago, Illinois<sup>3</sup> (1,021 fatalities), the 2003 European heat wave<sup>4</sup> (52,452 fatalities), the 2010 Russian event<sup>5,6</sup> (55,736 fatalities) and the 2011 event over the US Great Plains<sup>7</sup> (206 fatalities). Several studies identified that the effects of anthropogenic climate change (ACC) go beyond simple changes in the mean climate and include changes in the frequency and intensity of extremes<sup>8–10</sup> and noted that the number of heat waves and their severity have increased in recent decades<sup>11</sup>. In addition, there will probably be an increased exposure to heat extremes due to population growth<sup>12</sup>. Despite these findings, the impact of ACC on extreme weather, such as heat waves, is still not well understood<sup>13,14</sup>. This is especially true for the summer season due to the reduced synoptic variability over land<sup>15,16</sup>; a consensus has not been reached as to the mechanisms that link extreme events to ACC<sup>17–19</sup>. This study reports on the regional dependence and occurrence of heat waves over the United States with a focus on future projections and physical mechanisms that may accelerate or slow down the rate of occurrence of heat extremes under ACC.

The Fifth Assessment Report of the Intergovernmental Panel on Climate Change (IPCC) evaluated when the signal of ACC will emerge against the background natural variability<sup>20</sup> (that is, the time of emergence (ToE)) and found that for surface temperature, the ToE is regional dependent and occurs earlier for the warm season as well as for larger spatial and temporal scales. In contrast, most assessments of regional changes on heat waves associated with ACC are based purely on statistics, and the physical mechanisms that control the ToE for these extreme events are not yet understood fully. For example, the tails of the surface-temperature distributions appear to be sensitive to regional effects and may exhibit non-Gaussian behaviour, which may vary regionally, which suggests a need to verify the accuracy of climate models to simulate the

distribution tails<sup>21</sup>. Heat waves are linked to specific weather patterns that involve, for example, atmospheric circulation, precipitation deficits, soil moisture content and so on. Atmospheric high-amplitude planetary circulation patterns, such as lingering blocking patterns, are also associated with extreme heat wave events<sup>22</sup>.

To arrive at a more reliable projection of heat waves, it is important to describe these extreme events in a physical or phenomenological perspective. To do this, we focus on characterizing heat waves by clustering their spatial distribution and temporal structures. This method allows us to obtain the most-dominant spatial patterns of extremes, whereas more traditional methods, such as empirical orthogonal functions cannot guarantee the detection of individual dynamical modes due to the non-Gaussian distribution of the extremes<sup>23</sup>. The analysis of ensembles of models results in a purely empirical fashion will suffice for projection and attribution studies, but we have to account for the fact that these extremes are present without climate change and natural variability is a key component that modulates these extremes even under the most-pessimistic climate change scenario. Therefore, the identification of natural variabilities, how they may evolve and their implication on heat waves is essential to assess the risks of heat-related mortality given that natural variability is the main source of uncertainty in future projections.

The rareness of extreme events, the short observational record and the relative noisiness of mid-latitude atmospheric variability all contribute to making the study of heat waves difficult. To address this challenge, we use the European Center for Mid-Range Weather Forecast twentieth century reanalysis<sup>24</sup> (ERA-20C), multiple realizations of the Community Earth System Model (CESM1) Large Ensemble (LE) simulation<sup>25</sup> couple general circulation model and the Couple Model Intercomparison Project<sup>26</sup> (CMIP5) to examine heat waves in the United States, their modulation by internal climate variability versus external forcing and their non-stationary statistics in a climate change scenario. Supplementary Table 1 gives details on the models used.

<sup>1</sup>Cooperative Institute for Marine and Atmospheric Studies, University of Miami, Miami, FL, USA. <sup>2</sup>Atlantic Oceanographic and Meteorological Laboratory, NOAA, Miami, FL, USA. <sup>3</sup>Department of Earth, Ocean and Atmospheric Science, Florida State University, Tallahassee, FL, USA.

\*e-mail: [hlopez@rsmas.miami.edu](mailto:hlopez@rsmas.miami.edu)

Here we hypothesize that, although internal variability currently dominates the occurrence of heat waves in the United States, ACC will gradually assume a greater importance as we progress through the twenty-first century. However, the attribution of heat extremes due to ACC will vary by location. We quantify the time frame as to when ACC will dominate the occurrence of heat waves in the twenty-first century (that is, the ToE).

### Typical heat wave clusters over the United States

A hierarchical clustering algorithm (Methods) is applied to the daily mean surface temperature from the ERA-20C for the period 1900–2010. Eight major regional heat wave clusters are identified by the hierarchical algorithm (Supplementary Fig. 1). These clusters contain temperature anomalies well above  $5^{\circ}\text{C}$ , which affect large population areas. By definition, the clustering of heat waves allows us to separate each extreme event from other extremes that are synoptically independent and to investigate these clusters into physically coherent large-scale atmospheric patterns.

Here we focus on the four heat wave clusters that affect the largest portion of the US population; namely, the western United States, Northern Plains, Southern Plains and Great Lakes clusters (Table 1). The spatial structure of these four clusters is shown in Fig. 1. The cluster analysis was also repeated for the twenty-first century (Supplementary Fig. 2) using the CMIP5 models to test the robustness of these clusters under ACC and also for each of the CMIP5 model used (Supplementary Figs. 3–6). There is a positive trend in the daily mean summer temperature over each cluster region for the twenty-first century, consistent with the RCP8.5 scenario (Supplementary Fig. 7). There is also an increase in the ratio of warm-to-cold extreme temperature events, as shown in Table 1, column 7 (8), for the twentieth (twenty-first) century. These ratio changes are regionally dependent, with warm extremes that become significantly more likely for the Great Lakes and western United States cluster regions as compared to the Great Plains cluster regions shown in Table 1 (column 9). These changes in the asymmetry of extreme temperature, as well as their regional dependence, may have great implications for future projections of heat waves. It is, therefore, necessary to account not only for changes in the mean, but also for changes in the higher statistical moments (for example, variance, skewness and kurtosis) when considering the likelihood of heat wave events<sup>27</sup>.

### Natural variability and projection uncertainty

The recent apparent pause in warming of the climate system between approximately 1998 and 2014 has led to significant causal debate with respect to natural variability versus changes in external forcing<sup>28–30</sup>,

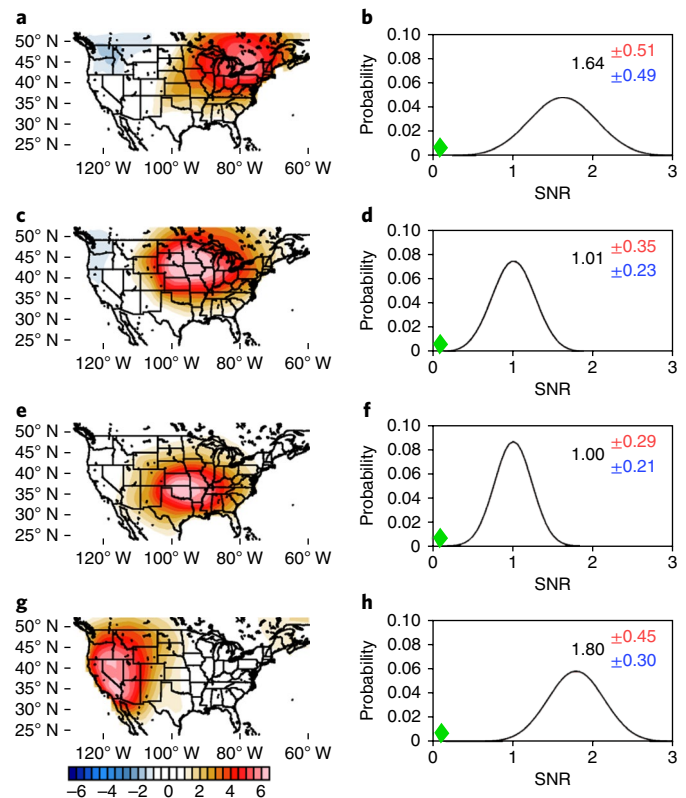


**Fig. 1 | Geographic distribution of heat waves.** **a, b**, Twentieth century 2 m temperature anomaly (**a**) and twenty-first century PDF of the SNR of heat wave events (**b**) for the Great Lakes cluster. **c–h**, Similarly, for the Northern Plains (**c** and **d**), Southern Plains (**e** and **f**) and western United States region (**g** and **h**) heat wave clusters from the ensemble mean of CMIP5 models. The SNR PDF is obtained by randomly selecting eight models (ensembles) 1,000 times from the CMIP5 (CESM1-LE) simulations. The mean SNR is shown in black and 95% confidence interval in red (blue) from the CMIP5 (CESM-LE). The twentieth century SNR is shown by green diamonds.

or even whether this pause is an artefact of observational biases<sup>31</sup>. Nevertheless, natural variability plays a key role in masking ACC at regional scales, because it influences the occurrence of extreme events and exacerbates the effects of anthropogenic forcing. It is, therefore, necessary to identify the mechanisms that affect the internal

**Table 1 | Statistics of summer 2 m air temperature extremes for the twentieth century (20C) and twenty-first century (21C) projections**

Cluster (population)	Mean 20C (21C) (27.5 ± 0.8)	Return period (years) of events $>3\sigma$				Ratios of events $>3\sigma$		
		20C PDF	21C PDF	20C PDF plus mean shift	21C PDF with no mean shift	Ratio of 20C warm to 20C cold	Ratio of 21C warm to 21C cold	Ratio 21C to warm to 20C warm
western United States (63,160,900)	23.2 ± 0.7 (27.5 ± 0.8)	376 ± 3	17 ± 14	60 ± 7	67 ± 6	0.6 ± 0.1	6.4 ± 0.6	2.1 ± 0.1
Northern Plains (46,843,000)	21.7 ± 0.4 (26.3 ± 0.7)	410 ± 3	17 ± 14	55 ± 7	65 ± 6	0.6 ± 0.1	1.7 ± 0.2	1.6 ± 0.1
Southern Plains (37,900,200)	23.4 ± 0.4 (27.4 ± 0.6)	404 ± 3	21 ± 12	68 ± 6	73 ± 6	0.7 ± 0.1	1.7 ± 0.2	1.6 ± 0.1
Great Lakes (78,935,400)	16.5 ± 0.4 (20.6 ± 0.6)	364 ± 3	20 ± 13	61 ± 7	70 ± 6	0.6 ± 0.1	10.2 ± 1.2	2.0 ± 0.1

Return periods are shown for the 20C, 21C, 20C plus mean changes (that is, shape-preserving distribution with no variance or higher moment changes) and 21C with no mean shift PDF (that is, the return period due solely to variance and higher moment changes). Uncertainty intervals ( $\pm$ ) correspond to the 99% confidence interval based on all 1,000 realizations of a Markov model. The eight-digit number beneath each cluster name indicates the population count affected by the cluster.

variability of heat waves, which is important for future mitigation and planning efforts.

Here we use the ensemble mean from the CMIP5 and CESM1-LE models as an estimate of the external forcing influence (signal), whereas the ensemble spread quantifies the internal component associated with a particular model ensemble member (noise). It is important to note that the contribution of internal variability to ensemble spread depends on the climate variable, season and location<sup>32</sup>. The number of heat wave days due to external forcing increases over the United States for near-future projections (that is, 2010–2100) when compared to previous periods for all heat wave clusters (Supplementary Fig. 10). The signal-to-noise ratio (SNR) of heat wave days for the twenty-first century (that is, 2020–2100) is significantly smaller for the Great Plains regions (Fig. 1d,f) compared to the Great Lakes and western United States regions (Fig. 1b,h), which indicates that future projection of heat waves over the Great Plains is more uncertain due to the large natural variability there.

The SNR shown in Fig. 1 is related to the ToE, which is dependent on the uncertainty in the climate response to external forcing and to the amplitude of the simulated internal variability<sup>33</sup>. Future projections show that external forcing will play a more dominant role, especially over the eastern and western thirds of the United States; however, the Great Plains region still shows a relatively large influence from internal variability. This is consistent with the concept that, at regional scales, internal variability is as important as ACC forcing, at least for the next half century<sup>32,34</sup>.

### Heat wave response to ACC

Future projections of heat waves are affected not only by changes in the mean temperature but also by changes in the extremes. It is, therefore, critical to quantify whether and to what extent non-stationary statistics affect these future projections. To address these issues, a stochastic generated skewed<sup>27</sup> (SGS) probability density function (PDF) of the summertime 2 m air temperature is quantified for each heat wave cluster depicted in Fig. 1 for the ERA-20C reanalysis, the CESM1-20C and CESM1-21C LE simulations (Methods). The summers include days from 1 June to 31 August, that is, a 92-day summer). The daily mean temperature and a 95th percentile threshold are used in the definition of heat waves (Methods). Figure 2 shows the SGS for each heat wave region. The CESM1-20C model reproduces the temperature distribution, including the negative skewness, of the ERA-20C reanalysis within all possibilities due to random error and uncertainty due to internal variability (Supplementary Fig. 8), which provides confidence in the model. ACC has no significant effect on the asymmetry of the SGS distribution for the Northern (Fig. 2a) and Southern (Fig. 2d) Plains regions. In contrast, the SGS distribution becomes significantly more positively skewed for the heat wave clusters over the Great Lakes (Fig. 2b) and western United States (Fig. 2c) regions, which suggests an increase in warm extremes. That is, the frequency of warm extremes is larger for the twenty-first century and significantly different (green shading) with respect to the twentieth century for the western United States and Great Lakes clusters.

The contrasting response of temperature anomalies over these heat wave regions is further investigated by analysing 1,000 realizations of a Markov model for the twentieth and twenty-first century CESM1 simulations (Methods). The increase in the number of warm extremes over the western United States and Great Lakes regions (that is, the ratio of 21C to 20C warm extremes of 2.1 and 2.0 respectively (Table 1)) is mostly due to a non-linear (asymmetric) response to changes in the mean and are influenced by anthropogenic forcing. In contrast, the modest increase in warm extremes over the two Great Plains regions (that is, the ratio of 21C to 20C warm extremes of 1.6 (Table 1)) is dominated by enhanced variability rather than by asymmetric changes (Supplementary Fig. 9).

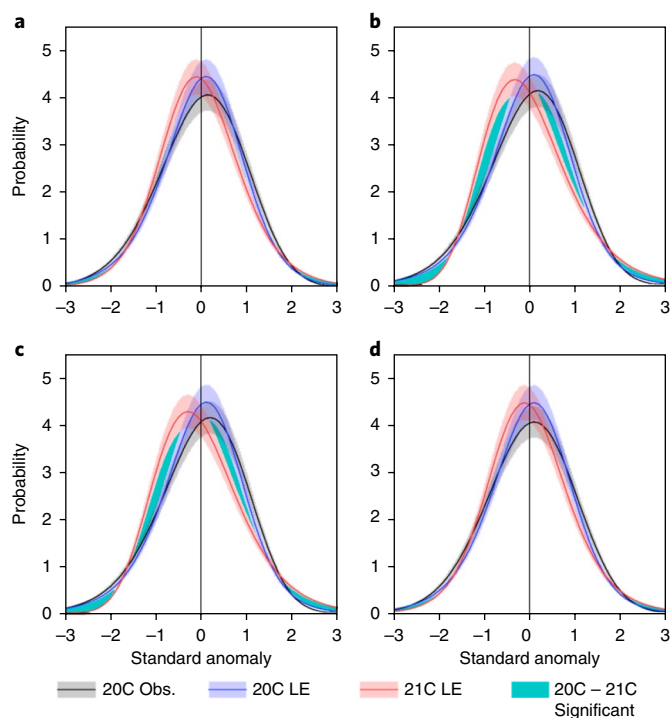


**Fig. 2 | SGS PDF of summertime 2 m temperature anomalies. a–d,** Northern Plains (a) Great Lakes (b), western United States (c) and Southern Plains (d) regions. The ERA-20C reanalysis for the 1920–2000 period is shown by black lines, the CESM1-20C (1920–2000) is shown as blue lines and the CESM1-21C (2020–2100) is depicted by the red lines. The spread depicted by the lighter colours represents the 99% confidence interval using all 1,000 realizations of the Markov model, which provides uncertainty due to random error. The green shading indicates statistically significant differences between the 20C and 21C PDFs at a 99% confidence level. Obs., observed.

These results demonstrate the need for caution in assessing and attributing heat waves due to changes in the mean climate related to ACC forcing as internal variability is large and also impacted by ACC, more notably over the Great Plains.

### Extreme event attribution, internal variability and ACC

Previous sections indicate the regional dependence of the relative role of internal variability and ACC on the modulation of heat extremes. This motivates the following question: if and/or when does ACC become significant with respect to heat extremes? To assess this, we quantify the probability of necessary causality ( $P_N$ ) for all heat extreme events in the twenty-first century projection (Methods). The  $P_N$  of each extreme event is drawn from the generalized Pareto (GP) distribution of summer temperature for each heat wave cluster (Fig. 3). The GP distribution for the twenty-first century is significantly distinct from that of the twentieth century for the western United States and Great Lakes heat wave clusters, and the uncertainty due to random error is greatly reduced in the twenty-first century. In contrast, the twentieth and twenty-first century GP distributions for the Great Plains heat waves (Fig. 3a,d) are not statistically well separated for high-threshold extremes (for example, a  $T > 3.5$  standard deviation).

Figure 4 shows the distribution of  $P_N$  values for the twenty-first century projection of heat extremes over each cluster. In general,  $P_N$  is projected to increase in the future, consistent with the RCP8.5 scenario. More importantly, each cluster has a distinctive evolution of  $P_N$ . For instance, ACC will be a necessary condition for at least half of the extreme events in the Northern Plains after the

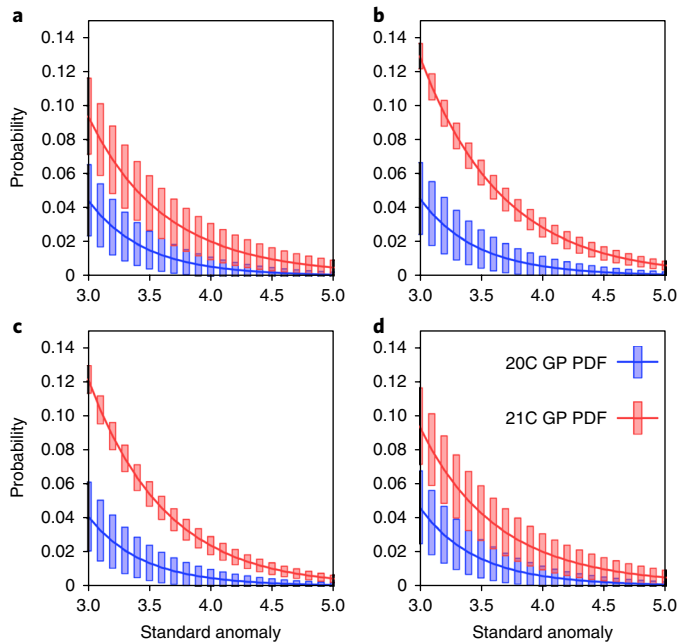


**Fig. 3 | GP distribution for the daily mean JJA standardized temperature anomalies.** Curves for the twentieth (blue) and twenty-first (red) centuries are shown. **a–d**, Northern Plains (**a**), Great Lakes (**b**), western United States (**c**) and Southern Plains (**d**) regions. The standard anomaly is derived by dividing the daily anomaly by the respective daily standard deviation. A standard anomaly is chosen for an easier comparison among regions. Vertical bars indicate the 99% range of uncertainty based on all 1,000 realizations of the Markov model.

year 2056 ± 2 (Fig. 4a), the Great Lakes after 2037 ± 1 (Fig. 4b), the Western region after 2028 ± 1 (Fig. 4c) and the Southern Plains not until 2074 ± 4 (Fig. 4d). These results show that heat extreme attribution to ACC is more certain for the western United States and Great Lakes regions. It also demonstrates that internal variability will be the dominant component of the Great Plains heat extreme occurrences well past the half-century mark. In fact, it is not until the late twenty-first century that increased heat waves due to ACC under the RCP8.5 scenario dominate internal variability over the Great Plains. This region also shows a smaller forced-to-internal ratio in the 50-year surface temperature trend<sup>35</sup>.

The attribution or necessary causation analysis shows that in the present climate, the fraction of heat extremes for which ACC plays a dominant role (that is,  $P_N > 0.5$ ) is still small for all regions. However, the influence of ACC is projected to increase significantly, and  $P_N > 0.1$  is already emerging (yellow regions in Fig. 4). For the western United States region (Fig. 4c), only 27 ± 2% of the heat extremes in the twenty-first century are projected to be entirely due to internal variability, whereas 23 ± 2% are projected to be caused predominantly by ACC. This is in contrast with heat extremes over the Southern Plains (Fig. 4d), where 62 ± 4% of extreme heat events are projected to be due to internal variability and only 8 ± 4% due to ACC, with a mix of both influences accounting for the remaining 30%.

### Sources of internal variability and uncertainty

Identifying the physical mechanisms that influence the internal variability of heat waves is necessary to improve projections, which leads to more-oriented mitigation and adaptation efforts. The atmospheric conditions associated with each heat wave cluster show a stationary anticyclone pattern located over the extreme warm temperature anomaly (Supplementary Fig. 11). Although all four clusters present negative precipitation anomaly patterns, only the two

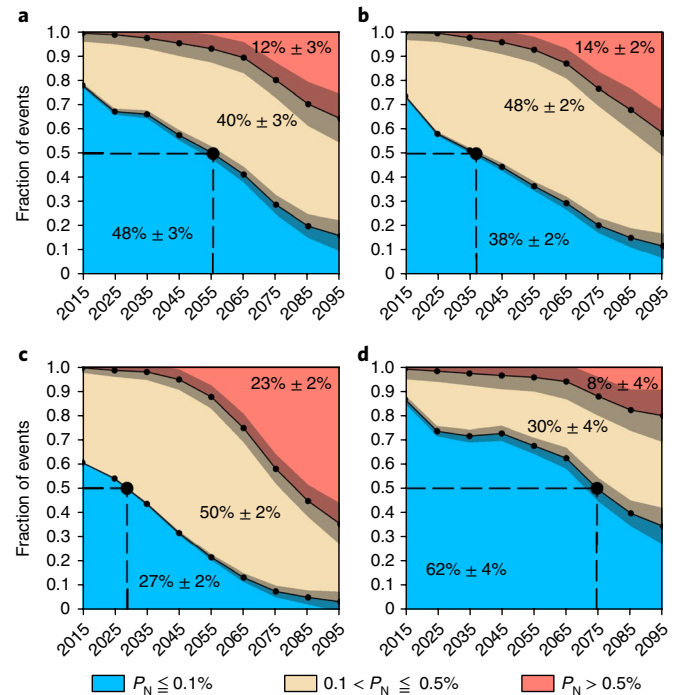


**Fig. 4 |  $P_N$  of heat waves. a–d**, Northern Plains (**a**), Great Lakes (**b**), western United States (**c**) and Southern Plains (**d**) regions.  $P_N$  values are binned into:  $P_N \leq 0.1$  (blue region, for example, ACC is not a necessary condition for heat waves),  $0.1 < P_N \leq 0.5$  (yellow, ACC is somewhat important) and  $P_N > 0.5$  (red, ACC is a necessary condition for heat waves). The intersection of the dashed lines denotes when ACC becomes a major contributor to heat extremes (that is, a measure of the ToE). The percentage values indicate the fraction of heat extremes attributed to each category. The ± value and the grey shading indicates a 95% confidence interval by randomly selecting 20 ensemble members 500 times.

Great Plains clusters depict coherent and large-amplitude drier conditions over the actual heat wave region.

There are two potential mechanisms by which changes in the mean climate can modulate the occurrence of extreme temperature events and heat waves. (1) Changes in atmospheric circulation as a result of the so-called Arctic amplification<sup>36,37</sup>. (2) Future changes in soil moisture, which influences surface temperature through the land–atmosphere feedback<sup>38,39</sup>. For instance, atmospheric transient eddies (storminess) are strongly negatively correlated with surface temperature over the western and northeastern United States (Fig. 5a), which suggests that less storminess is linked to warmer surface temperatures. In addition, storm activities over these same regions are projected to decrease significantly for the twenty-first century (Fig. 5b) due to meridionally asymmetric warming<sup>40</sup>. In contrast, the Great Plains is in a transitional hydrological regime in which soil moisture is a limiting constraint on evapotranspiration and latent heating, which influences climate variability through coupling and feedbacks with the atmosphere<sup>41,42</sup>. Here, more precipitation leads to more soil moisture, which decreases surface air temperature. Also, due to the strong coupling and feedbacks between air temperature and soil moisture, an enhanced variability in precipitation and soil moisture will lead to an enhanced variability in surface temperature through latent heating, which adds uncertainty to future projections of heat extremes.

The question of why the Great Plains events appear to be less sensitive to ACC than those from the western United States and Great Lakes clusters is addressed in Fig. 5. The June–July–August (JJA) climatological near-surface (925 hPa) wind shown in Fig. 5c for the

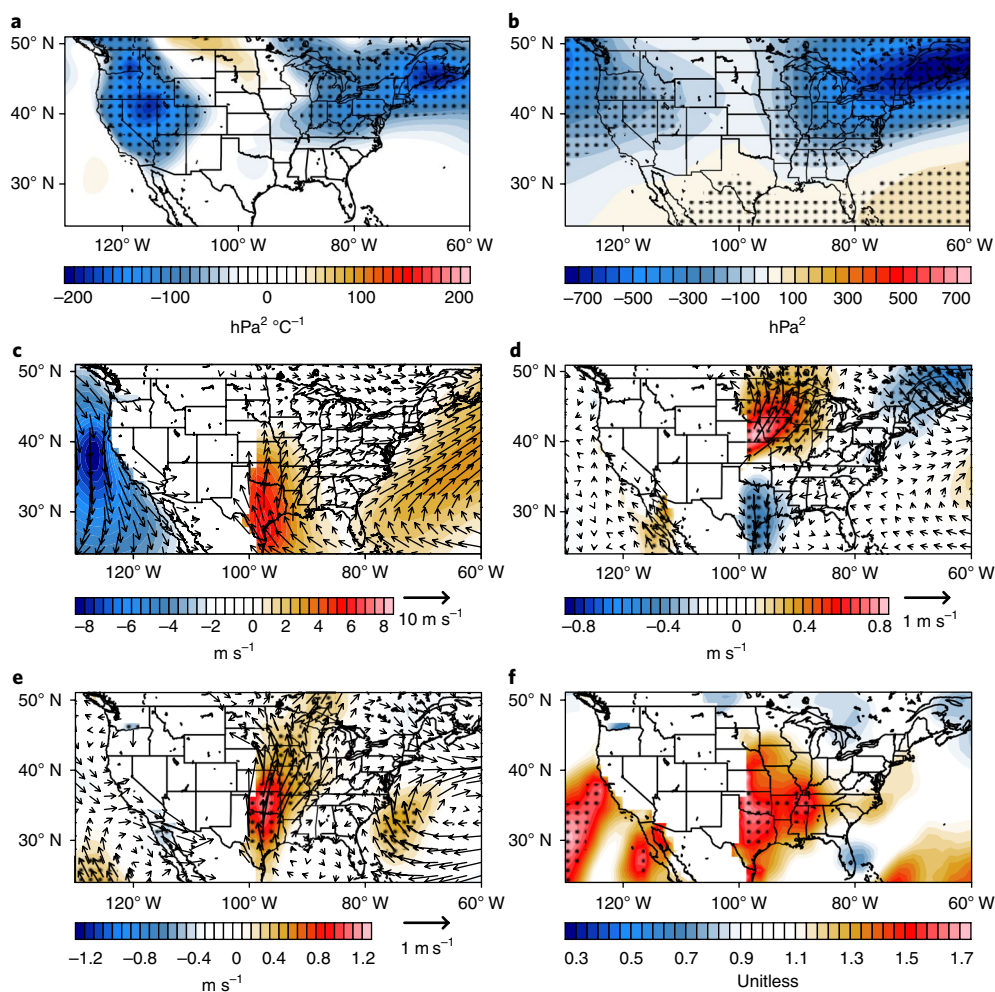


**Fig. 5 | Great Plains low-level jet and heat waves.** **a**, Regression of JJA transient eddies and 2 m temperature ( $\text{hPa}^2 \text{ } ^\circ\text{C}^{-1}$ ). **b**, Projected changes of JJA transient eddies ( $\text{hPa}^2$ ). **c**, CMIP5 ensemble mean JJA 925 hPa wind (vector) and meridional wind (colour) from the historical period. **d**, Same as **c**, but for the composite during Northern and Southern Great Plains heat waves from the historical period. **e**, Same as **c**, but twenty-first minus twentieth century JJA 925 hPa winds. **f**, Variance ratio of twenty-first to twentieth century JJA 925 hPa meridional wind. The stipples in **a–d** and **f** indicate the 95% level based on a student-*t* test and an *F*-test, respectively.

twentieth century CMIP5 ensemble mean depicts a strong southerly flow from the Gulf of Mexico towards the Great Plains, known as the Great Plains low level jet (GPLLJ). The GPLLJ is responsible for about one-third of the total moisture transport into the Great Plains, and affects precipitation<sup>43–46</sup>. The strength of the GPLLJ is positively correlated to the moisture transport in the Great Plains (Supplementary Fig. 12) and leads to more precipitation in the Great Plains. In these regions, precipitation is strongly coupled to soil moisture<sup>41</sup>, and therefore changes in precipitation associated with the GPLLJ should impact soil moisture and thus surface temperature.

There is currently a positive trend in the precipitation over the Great Plains for the spring and summer<sup>47,48</sup>, caused by the strengthening of the GPLLJ<sup>49</sup>. In the CMIP5 models, the GPLLJ is also projected to increase (Fig. 5e), as previously found in another study<sup>50</sup>, caused by differential heating between land and the adjacent ocean<sup>51</sup>. We also found a strong negative correlation between projected changes in the GPLLJ amplitude and projected changes in the number of heat wave days among CMIP5 models (Supplementary Fig. 13). This suggests that an enhanced GPLLJ can lead to fewer heat extremes. On the other hand, the presence of a heat wave in the Great Plains can weaken the GPLLJ due to circulation anomalies, as shown in Fig. 5d, but this is beyond the scope of this study. The variability of the GPLLJ is also projected to increase (Fig. 5f), which

suggests an enhanced uncertainty in future projections of soil moisture and thus surface temperature. Also, an increase in the GPLLJ amplitude should enhance the land–atmosphere feedback as this is a region in which soil moisture is a limiting factor for latent heat flux.

In all, the enhanced GPLLJ and moisture transport due to ACC serves to attenuate the anomalous negative (northerly) wind often present during heat wave events and which depletes soil moisture. The strong land–atmosphere feedback over the Great Plains along with the projected enhanced variability of the GPLLJ suggests that the future projection of heat extremes in the Great Plains is more uncertain and masked by a large internal variability (Supplementary Fig. 14). It can be said that an enhanced GPLLJ could help alleviate some of the effects of temperature increase due to ACC. This is not the case for the western United States and Great Lakes heat wave clusters, where the projected significant reduction of atmospheric transient eddies ensures a robust increase in warm-temperature extremes on top of the mean climate shift, as shown by the relatively earlier ToE in those regions. Therefore, attributions of heat extremes to ACC in these regions is more certain, as shown by the attribution analysis (Fig. 4). These results hint at the need for caution in attributing heat extremes to changes in the mean, given that the relationship of mean climate shifts and their modulation on the higher statistical moments are non-linear and regional in nature. Our study

emphasizes that the consequences of increased heat wave amplitude and frequency in the Great Lakes and western United States could be further exacerbated by the large population and rapid population increase in these regions, which highlights the regions where mitigation and adaptation efforts are most required.

## Methods

Methods, including statements of data availability and any associated accession codes and references, are available at <https://doi.org/10.1038/s41558-018-0116-y>.

Received: 25 April 2017; Accepted: 20 February 2018;

Published online: 19 March 2018

## References

- Wolfson, N. & Atlas, R. A simple diagnostic tool for the investigation of persistent phenomena with applications to the summer 1980 U.S. heat wave. *Atmos. Ocean* **24**, 111–127 (1986).
- Meehl, G. A. & Tebaldi, C. More intense, more frequent, and longer lasting heat waves in the 21st century. *Science* **305**, 994–997 (2004).
- Karl, T. R. & Knight, R. W. The 1995 Chicago heat wave: how likely is a recurrence? *Bull. Am. Meteorol. Soc.* **78**, 1107–1119 (1997).
- Schär, C. et al. The role of increasing temperature variability in European summer heat waves. *Nature* **427**, 332–336 (2004).
- Dole, R. et al. Was there a basis for anticipating the 2010 Russian heat wave? *Geophys. Res. Lett.* **38**, L06702 (2011).
- Trenberth, K. E. & Fasullo, J. T. Climate extremes and climate change: the Russian heat wave and other climate extremes of 2010. *J. Geophys. Res.* **117**, D17103 (2012).
- Hoerling, M. Anatomy of an extreme event. *J. Clim.* **26**, 2811–2832 (2013).
- IPCC *Climate Change 2007: Mitigation of Climate Change* (eds Metz, B., Davidson, O. R., Bosch, P. R., Dave, R. & Meyer, L. A.) (Cambridge Univ. Press, 2008).
- Duffy, P. B. & Tebaldi, C. Increasing prevalence of extreme summer temperatures in the US. *Climatic Change* **111**, 487–495 (2012).
- Khari, V. V., Zwiers, F. W., Zhang, X. & Wehner, M. Changes in temperature and precipitation extremes in the CMIP5 ensemble. *Climatic Change* **119**, 345–357 (2013).
- Karl, T. R. & Quayle, R. P. The 1980 summer heat wave and drought in historical perspective. *Mon. Weather Rev.* **109**, 2055–2073 (1981).
- Jones, B. & et al. Future population exposure to US heat extremes. *Nat. Clim. Change* **5**, 652–655 (2015).
- Kim, O.-Y., Wang, B. & Shin, S.-H. How do weather characteristics change in a warming climate? *Clim. Dynam.* **41**, 3261–3281 (2013).
- Cattiaux, J., Douville, H., Schoetter, R., Parey, S. & Yiou, P. Projected increase in diurnal and interdiurnal variations of European summer temperatures. *Geophys. Res. Lett.* **42**, 899–907 (2015).
- Schneider, Tapio, Bischoff, Tobias, & Plotka, Hanna. Physics of changes in synoptic midlatitude temperature variability. *J. Clim.* **28**, 2312–2331 (2015).
- Screen, J. A. Arctic amplification decreases temperature variance in northern mid- to high-latitudes. *Nat. Clim. Change* **4**, 577–582 (2014).
- Palmer, T. N. Climate extremes and the role of dynamics. *Proc. Natl Acad. Sci. USA* **110**, 5281–5282 (2013).
- Shepherd, T. G. Atmospheric circulation as a source of uncertainty in climate change projections. *Nat. Geosci.* **7**, 703–708 (2014).
- Teng et al. Projected intensification of subseasonal temperature variability and heat waves in the Great Plains. *Geophys. Res. Lett.* **43**, 2165–2173 (2016).
- Kirtman, B. P. & Power, S. B. in *Climate Change 2013: The Physical Science Basis* (eds Stocker, T. F. et al.) Ch. 11 (IPCC, Cambridge Univ. Press, 2014).
- Ruff, T. W. & Neelin, J. D. Long tails in regional surface temperature probability distributions with implications for extremes under global warming. *Geophys. Res. Lett.* **39**, L04704 (2012).
- Petoukhov, V., Rahmstorf, S., Petri, S. & Schellnhuber, H. J. Quasiresonant amplification of planetary waves and recent Northern Hemisphere weather extremes. *Proc. Natl Acad. Sci. USA* **110**, 5336–5341 (2013).
- Monahan, A. H., Fyfe, J. C., Ambaum, M. H. P., Stephenson, D. B. & North, G. R. Empirical orthogonal functions: the medium is the message. *J. Clim.* **22**, 6501–6514 (2009).
- Poli, P. et al. ERA-20C: an atmospheric reanalysis of the twentieth century. *J. Clim.* **29**, 4083–4097 (2016).
- Kay, J. E. The Community Earth System Model (CESM) large ensemble project: A community resource for studying climate change in the presence of internal climate variability. *Bull. Am. Meteorol. Soc.* **8**, 1333–1349 (2015).
- Taylor, K. E., Stouffer, R. J. & Meehl, G. A. An overview of CMIP5 and the experiment design. *Bull. Am. Meteorol. Soc.* **93**, 485–498 (2012).
- Sardeshmukh, D. P., Compo, G. P. & Penland, C. Need for caution in interpreting extreme weather statistics. *J. Clim.* **28**, 9166–9187 (2015).
- Tollefson, J. The case of the missing heat. *Nature* **505**, 276–278 (2014).
- Solomon, S. et al. The persistently variable 'background' stratospheric aerosol layer and global climate change. *Science* **333**, 866–870 (2011).
- Clement, A. & DiNezio, P. The tropical Pacific Ocean—back in the driver's seat? *Science* **343**, 976–978 (2014).
- Karl, T. R. et al. Possible artifacts of data biases in the recent global surface warming hiatus. *Science* **348**, 1469–1472 (2015).
- Deser, C., Knutti, R., Solomon, S. & Phillips, A. S. Communication of the role of natural variability in future North American climate. *Nat. Clim. Change* **2**, 775–779 (2012).
- Hawkins, E. & Sutton, R. Time of emergence of climate signals. *Geophys. Res. Lett.* **39**, L01702 (2012).
- Wallace, J. M., Deser, C., Smoliak, B. V. & Phillips, A. S. in *Climate Change: Multidecadal and Beyond* (ed. Chang, C.-P.) 1–29 (World Scientific Series on Asia-Pacific Weather and Climate Vol 6, World Scientific, Singapore 2013).
- Deser, C., Phillips, A. S., Alexander, M. A. & Smoliak, B. V. Projecting North American climate over the next 50 years: uncertainty due to internal variability. *J. Clim.* **27**, 2271–2296 (2014).
- Barnes, E. A. & Screen, J. A. The impact of Arctic warming on the midlatitude jet stream: Can it? Has it? Will it? *WIREs Clim. Change* **6**, 277–286 (2015).
- Coumou, D., Lehmann, J. & Beckmann, J. The weakening summer circulation in the Northern Hemisphere mid-latitude. *Science* **348**, 324–327 (2015).
- Koster, R. D. et al. Regions of strong coupling between soil moisture and precipitation. *Science* **305**, 1138–1140 (2004).
- Fischer, E. M., Rajczak, J. & Schär, C. Changes in European summer temperature variability revisited. *Geophys. Res. Lett.* **39**, K19702 (2012).
- Lehmann, J., Coumou, D., Frieler, K., Eliseev, V. & Livermann, A. Future changes in extratropical storm tracks and baroclinicity under climate change. *Environ. Res. Lett.* **9**, 084002 (2014).
- Koster, R. D. et al. GLACE: The Global Land–Atmosphere Coupling Experiment. Part I: overview. *J. Hydrometeorol.* **7**, 590–610 (2006).
- Seneviratne, S. I. et al. Investigating soil moisture–climate interactions in a changing climate: a review. *Earth Sci. Rev.* **99**, 125–161 (2010).
- Walters, C. K. & Winkler, J. A. Airflow configurations of warm season southerly low-level wind maxima in the Great Plains. Part I: Spatial and temporal characteristics and relationship to convection. *Weather Forecast.* **16**, 513–530 (2001).
- Wexler, H. A boundary layer interpretation of the low level jet. *Tellus* **13**, 368–378 (1961).
- Jiang, X., Lau, N.-C., Held, I. M. & Ploshay, J. J. Mechanisms of the Great Plains low-level jet as simulated in an AGCM. *J. Atmos. Sci.* **64**, 532–547 (2007).
- Cook, K. H., Vizi, E. K., Launer, Z. S. & Patricola, C. M. Springtime intensification of the Great Plains low-level jet and Midwest precipitation in GCM simulations of the twenty-first century. *J. Clim.* **21**, 6321–6384 (2008).
- Kunkel, K. E. et al. Monitoring and understanding trends in extreme storms: state of knowledge. *Bull. Am. Meteorol. Soc.* **94**, 499–514 (2013).
- Janssen, E., Wuebbles, D. J., Kunkel, K. E., Olsen, S. C. & Goodman, A. Observational- and model-based trends and projections of extreme precipitation over the contiguous United States. *Earth's Future* **2**, 99–113 (2014).
- Feng, Z. et al. More frequent intense and long-lived storms dominate the springtime trend in central US rainfall. *Nat. Commun.* **7**, 13429 (2016).
- Tang, Y. et al. Future changes in the climatology of the Great Plains low-level jet derived from fine resolution multimodel simulations. *Sci. Rep.* **7**, 5029 (2017).
- Cook, K. H., Vizi, E. K., Launer, Z. S. & Patricola, C. M. Springtime intensification of the Great Plains low-level jet and midwest precipitation in GCM simulations of the twenty-first century. *J. Clim.* **21**, 6321–6340 (2008).

## Acknowledgements

We acknowledge D. Enfield, G. Foltz (NOAA/AOML), E. Johns (NOAA/AOML) and G. Derr (NOAA/AOML) for their comments and suggestions that greatly improved the manuscript. This research was carried out in part under the auspices of the Cooperative Institute for Marine and Atmospheric Studies, a cooperative institute of the University of Miami and the National Oceanic and Atmospheric Administration (NOAA), cooperative agreement NA10OAR4320143. This work was funded by NOAA's Atlantic Oceanographic and Meteorological Laboratory and by the Climate Observations Division of the NOAA Climate Program Office. S.D. acknowledges funding by NASA grant NNH13AW331. H.L. acknowledges funding from NOAA Climate Program Office CVP program (GC16-208). S.-K.L. acknowledges funding from NOAA Climate Program Office CVP program (GC16-207). B.P.K. acknowledges funding from the US National Science Foundation (OCE1419569).

**Author contributions**

H.L. conceived the study, designed and performed the statistical analysis and wrote the initial draft of the paper. H.L., R.W., S.D., S.-K.L., G.G., B.K. and R.A. contributed to the discussion and interpretation of the results as well as to the writing of the final version of the paper.

**Competing interests**

The authors declare no competing interests.

**Additional information**

**Supplementary information** is available for this paper at <https://doi.org/10.1038/s41558-018-0116-y>.

**Reprints and permissions information** is available at [www.nature.com/reprints](http://www.nature.com/reprints).

**Correspondence and requests for materials** should be addressed to H.L.

**Publisher's note:** Springer Nature remains neutral with regard to jurisdictional claims in published maps and institutional affiliations.

## Methods

**Models and observational data sets.** The ERA-20C reanalysis is used as an estimate of historical heat wave occurrence over the United States and to assess the fidelity of the CESM1-LE and the CMIP5 models in reproducing the spatial patterns of heat waves. A multi-century pre-industrial run from CESM1-LE is used to quantify heat wave statistics in the absence of anthropogenic forcing. CESM1-LE and CMIP5 model simulations under twentieth century and the Representative Carbon Path 8.5 (RCP8.5) future scenario are analysed for heat waves under external forcing. The CESM1-LE simulation provides a LE size from a single model; consequently, the ensemble spread is solely due to internal climate variability<sup>25</sup>, whereas the CMIP5 simulations provide a multi-model ensemble approach aimed to reduce model errors by ensemble averaging. We analysed a 1,000-year pre-industrial simulation (CESM1-PI) with constant 1850 forcing as the basis for the internal variability of the heat waves, a 30-member ensemble simulation (CESM1-LE) for the period 1920–2100 and multiple CMIP5 models for the period 1920–2100. Each model simulation has a distinct climate trajectory due to differences in the atmospheric initial conditions. All the models have the same specified external forcing, with historical forcing from 1920 to 2005 and RCP8.5 forcing<sup>52,53</sup> from 2006 to 2100 following the CMIP5 design protocol.

**Heat wave cluster.** The definition of heat wave proposed here is based on clustering of the daily mean temperature that covers each summer from 1 June to 30 August<sup>54</sup>. For a temperature extreme to qualify as a heat wave, it must satisfy the following three constraints:

**Threshold anomaly.** For each day and grid point, a temperature anomaly with respect to the daily mean climatology is defined. The daily mean climatology is smoothed with a 20-day running average. The 20-day smoothing of the daily climatology is performed to account for the synoptic variability of typical extreme heat anomalies. Extremes are defined as anomalies larger than the 95th percentile threshold.

**Spatial smoothing.** A spatial filter is applied to the threshold anomalies to eliminate the influence of small-scale extremes (that is, hot grid points). Each grid point is used as the centre of a square of size  $L$ . A sliding scan is performed, and only those points for which the fraction of threshold anomalies exceeds some ratio  $\alpha$  are retained. The number of grid points (that is, stations) within the  $L^2$  region depends on the resolution of the temperature data.  $L$  was chosen so that the sliding scan has a horizontal resolution of about  $4^\circ$  in latitude and longitude. We tested the sensitivity of this parameter from  $2^\circ < L < 6^\circ$  without much change in the distribution of the clusters nor in the dissimilarity index.

**Temporal smoothing.** The criteria for items (1) and (2) must be met for a minimum of three consecutive days to exclude short-duration events, which are uncharacteristic of synoptic and planetary scale heat waves. Propagating events are accounted for by merging events with overlapping areas of more than 40% during the three-day window.

Events that satisfied the above three constraints were considered to be heat wave events. These events were clustered using a hierarchical clustering algorithm<sup>54–56</sup>, which was previously applied to European heat waves<sup>54</sup>. The clustering algorithm comprises the following three steps (1)–(3):

- (1) For each event map, temperature anomalies that do not satisfy the previous three constraints are set to zero, and those that do satisfy the three constraints are retained. In the case of heat waves, all the anomalies are positive by definition.
- (2) All maps that belong to a specific event are merged into a single event. That is, a single heat wave event includes several daily temperature-anomaly maps that are averaged into a single heat wave. Therefore, each heat wave event is an independent cluster.
- (3) The agglomerative hierarchical clustering algorithm is applied to the clusters defined in step (5). The algorithm quantifies the intercluster distance between two clusters  $M$  and  $N$  using equation (1). The two closest clusters are merged into a single new cluster. This procedure is repeated until a stop criterion is met, which sets the final number of clusters:

$$d(M, N) = 1 - \frac{\sum_{i=1}^I \sum_{j=1}^J M_{ij} N_{ij}}{\left[ \sum_{i=1}^I \sum_{j=1}^J M_{ij}^2 \right]^{1/2} \left[ \sum_{i=1}^I \sum_{j=1}^J N_{ij}^2 \right]^{1/2}} = 1 - r(M, N) \quad (1)$$

Here,  $r(M, N)$  is the spatial correlation of clusters  $M$  and  $N$  over all grid points  $I$  and  $J$ . The intercluster distance is taken as the average distance between all the members of clusters  $M$  and  $N$ . The dissimilarity index, equation (1), provided the optimum number of clusters, which was found to be eight clusters.

**SGS PDF.** For each heat wave cluster, we assess changes in the PDF of summer temperature extremes by modelling the PDF as a SGS distribution<sup>27</sup>. The SGS of a

variable  $X$  is defined in equation (2), where  $E$ ,  $g$ ,  $b$  and  $N$  are parameters obtained from the statistical moments of  $X$ :

$$\text{SGS}(X) = \frac{1}{N} [(EX + g)^2 + b^2]^{-1 + (1/E^2)} \exp \left[ \frac{2g}{E^2 b} \tan^{-1} \left( \frac{EX + g}{b} \right) \right] \quad (2)$$

A Markov model<sup>27</sup> for the variable  $X_t$  is defined in equation (3) using the same parameters as for the SGS distribution. The model is damped and forced by cumulative additive  $(b\eta_1 + g\eta_2)$  and multiplicative  $(EX_t)\eta_2$  noise, where  $\eta_1$  and  $\eta_2$  are random Gaussian variables with a zero mean and unit variance. Equation (3) is integrated forward using a fourth-order Runge–Kutta method, with a time step ( $dt = 1$  hour) and decorrelation time scale ( $\lambda = 4$  days) to produce 81 summers of 92-day length. This process is repeated 1,000 times for a total of 1,000 time series of 7,452-day length, which is the same length of the 1920–2000 and 2020–2100 summer periods for the twentieth and twenty-first centuries used here:

$$X_{t+1} = X_t - \left[ \left( 1 + \frac{E^2}{2} \right) X_t + \frac{Eg}{2} \right] \lambda dt + [b\eta_1 + (EX_t + g)\eta_2] \sqrt{\lambda dt} \quad (3)$$

This approach allows us to quantify the non-Gaussian aspect of the meteorological fields (for example, surface temperature for our purpose). The modelling of 2 m temperatures using the SGS approach brings several main benefits. First, it provides a means to quantify the influence of climate shifts under Gaussian and non-Gaussian assumptions. Second, it enables us to investigate how changes in climate influence the statistical moments of summer temperature and its PDF. Finally, the parameters of the SGS distribution can be used to define the shape and scale parameters of the extreme value GP distribution<sup>27</sup>. The Markov model is also used to assess confidence interval for the GP distribution due to random errors.

$P_N$ . Here,  $P_N$  is the fraction of extreme events attributed to ACC, defined as:

$$P_N = \max \left\{ 1 - \frac{P_0}{P_1}, 0 \right\} \quad (4)$$

where  $P_0$  is the probability of an event occurring in the counterfactual world (that is, without ACC) and  $P_1$  is the probability of that same event occurring in the factual world (that is, including ACC).  $P_N$  ranges from zero to one and indicates whether ACC is a necessary condition for the extreme event to occur. That is, the extreme event would not occur in the absence of ACC. The probabilities  $P_0$  and  $P_1$  are obtained from a GP distribution of the pre-industrial and twenty-first century summer temperatures, respectively.

Given that extreme events are by definition rare,  $P_N$  is quantified using all heat extremes in all 30 ensembles of the twenty-first century run. Then, for each decade, all  $P_N$  values are binned into three groups:  $P_N \leq 0.1$  (ACC is not a necessary condition for most heat extremes),  $0.1 < P_N \leq 0.5$  and  $P_N > 0.5$  (ACC is a necessary condition for more than half of the temperature extremes). For example, a distribution of  $P_N$  that spans the summers of 2010–2019 and all 30 ensembles for a total of 300 summers is quantified. This is repeated for all decades, which allows for a representative sample size of heat extremes. The results are presented in Fig. 4 as a probability plot of  $P_N$  values for each decade and bin. This allows us to make assessments of heat extreme attribution to ACC into the future.

**Transient eddies (storminess) definition.** Transient eddies are defined as the square of the departure from the monthly mean of daily mean geopotential height at 500 hPa.

**Data availability.** The data that support the findings of this study are available from the corresponding author upon request.

## References

52. Meinhausen, M. The RCP greenhouse gas concentration and their extension from 1765 to 2300. *Climatic Change* **109**, 213 (2011).
53. Lamarque, J. F. Global and regional evolution of short-lived radiatively-active gases and aerosols in the Representative Concentration Pathways. *Climatic Change* **109**, 191–212 (2011).
54. Stefanon, M., Fabio, D. & Drobninski, P. Heat wave classification over Europe and the Mediterranean region. *Environ. Res. Lett.* **7**, 014023 (2012).
55. Smyth, P., Ide, K. & Ghil, M. Multiple regimes in Northern Hemisphere height fields via mixture model clustering. *J. Atmos. Sci.* **56**, 3704–3723 (1999).
56. Tan, P. N., Steinbach, M. & Kumar, V. *Introduction to Data Mining* (Addison-Wesley, Reading, MA, 2006).